Hindawi
Advances in Civil Engineering
Volume 2023, Article ID 8862459, 14 pages
https://doi.org/10.1155/2023/8862459

Research Article

A Novel Coal Burst Criterion of Anchored Roadway Surrounding Rock under Dynamic Disturbance

Zheng-yi Wang and Peng-bo Li

School of Civil Engineering and Architecture, Changzhou Institute of Technology, Changzhou, Jiangsu 213032, China

Correspondence should be addressed to Zheng-yi Wang; 15062193699@163.com

Received 9 June 2023; Revised 17 September 2023; Accepted 21 October 2023; Published 9 November 2023

Academic Editor: Prabhat Kumar Mandal

Mining roadway is the main occurrence area of coal bursts in underground coal mining. A good understanding of the failure process of elastic zone and energy evolution inducing instability of support structure can offer useful insight into the coal burst mechanism. This study proposes a novel coal burst criterion of anchored roadway surrounding rock under dynamic disturbance through mechanical modeling. The coal burst hazard and its main controlling factors were studied based on case analysis, and then the application of novel criterion in coal burst prevention and control was clarified. Results show that the existence of residual energy U_r of elastic zone is a prerequisite for coal burst of the roadway. The roadway support with ultimate value U_s of absorbed energy needs to resist and absorb the kinetic energy U_k released from a dynamic failure of elastic zone and the energy U_p imposed by impact-induced convergence of surrounding rocks on a support system, and the novel coal burst criterion is proposed as $U_k + U_p > U_s$. Under the same support conditions, the roadway roof is more prone to dynamic failure. According to the influences of main controlling factors on coal burst hazard, the corresponding prevention and control measures can be taken from improvement for the anti-impact capability of support, pressure relief in surrounding rocks, reduction of dynamic-loading energy, and roadway restoration after coal burst.

1. Introduction

Coal burst is one of the most serious dynamic disasters in underground coal mining [1]. With the increase in mining depth, coal burst disasters have been widely reported worldwide, including in Poland [2, 3], Russia [4], the United States [5], Canada [6], France [7], China [8, 9], and Australia [10, 11]. Coal bursts have both occurred in working face and mining roadway, but mainly in the latter, accounting for 91% of the total times of coal bursts [12]. The additional dynamic disturbance caused by mining-induced seismicity is the main contributor to triggered coal bursts of roadway [13, 14].

As for the coal burst of anchored roadway under dynamic disturbance, many scholars have conducted abundant researches on its mechanism and criterion and gained fruitful achievements. Wang et al. [15] investigated the dynamic responses of circular anchored roadways under P-wave loading, which indicated that roadway surrounding rocks exhibited regional differences in deformation and bearing capacity when the roadway was subjected to dynamic loading from one side. Song et al. [16] established a dynamic ejection coal burst model for a coalmine roadway subject to stress and held that the stress concentration zone at the roadway side is the direct energy source of this ejection. Zhang and Jiang [17] evaluated the abutment stress applied to the roadway surrounding rock by constructing an abutment-stress-transfer model and proposed the stress criterion and energy criterion for coal burst occurrence according to roadway types. Dai et al. [18] established a mechanical model for coal bursts and obtained critical indexes of the surrounding rock fracture and coal burst occurrence by involving seismic disturbance factors with in situ stress, mechanical properties of the coal and rock mass, support strength, and roadway size. Gao et al. [19] established a strong-soft-strong (3S) mechanical model for stability control of roadway surrounding rock under coal bursts. The 3S structure showed significant regional characteristics in strength, stress transfer, deformation, and energy dissipation, which can be reasonably designed to prevent coal

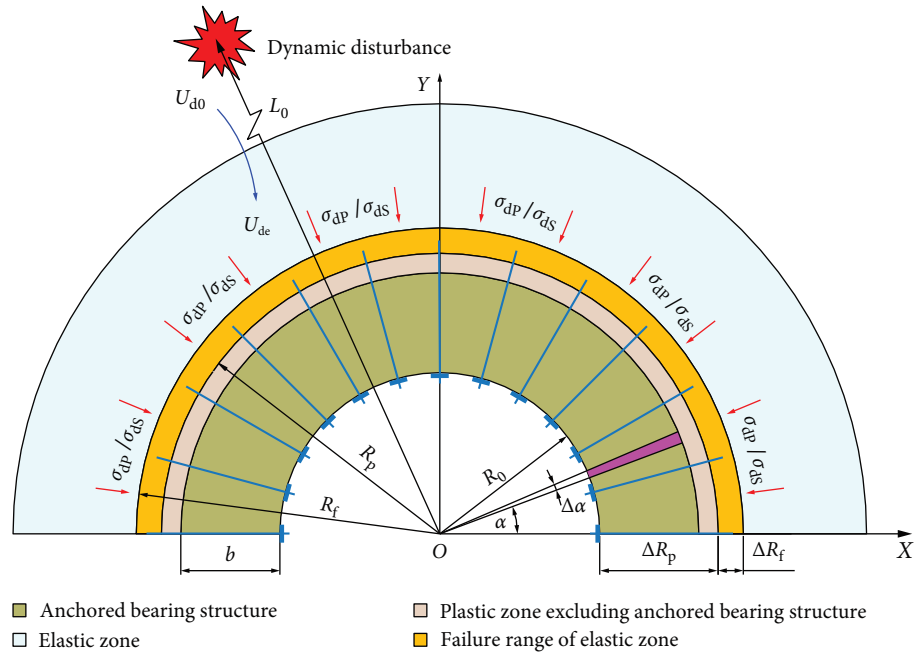

Figure 1: Mechanical analysis model for bearing structure of roadway surrounding rock under dynamic loading.

bursts. Jiao and Ju [20] established a mechanical and energy model for bearing structure stability of anchored roadway under the superposition of dynamic and static loads, and the mechanical and energy criterion for impact failure of bearing structures induced by dynamic disturbance were obtained. Vardar et al. [21] developed a practical approach to quantitatively estimate coal burst proneness in development roadways by establishing a novel burst proneness rating system based on energy release characteristics.

The studies mentioned above have enhanced our understanding of coal bursts of roadway under dynamic disturbance. The failure mechanisms in most previous studies are revealed based on the premise that the dynamic load directly acts on entire anchored surrounding rocks. However, during the bursting process, the surrounding rocks of elastic zone first undergo failure and release energy, which is crucial for impact damages and needs to be further studied. In addition, energy sources inducing instability of support structure and their evolution also need to be analyzed.

In this study, considering the impact failure process and corresponding energy evolution, a mechanical analysis model for the bearing structure of roadway surrounding rock under dynamic loading was built to propose a novel coal burst criterion. Then, the coal burst hazard and influences of the main controlling factors were analyzed through a case study, which were verified in practice. Finally, the application of this novel criterion in coal burst prevention and control was discussed.

2. Mechanical Modeling Method

2.1. Establishment of Model. Taking the typical semicircular arched roadway in underground coal mining as the research object, a mechanical analysis model for the bearing structure of roadway surrounding rock under dynamic loading was built, as shown in Figure 1. In order to simply the calculation, the following assumptions were proposed: (1) the roadway surrounding rock was homogeneous and isotropous, without creep and viscous behaviors; (2) the original rock stress was in a hydrostatic pressure state; (3) the buried depth of roadway was far larger than the roadway size; (4) the cross-section of roadway was semicircular and regarded as a plane-strain model with the axial length of 1; (5) the distance from dynamic disturbance to roadway center O was L_0. In addition, the propagation regulation of vibration waves in surrounding rocks conformed to that in elastic media. Because the dynamic disturbance was generally caused by the fracture of higher thick-hard rock strata under mining, the disturbance source was far away from the roadway space [19]. In Figure 1, the relationship between L_0 and roadway radius R_0 was usually one to two or even greater orders of magnitude, namely that the roadway size was very small relative to the propagation scope of dynamic disturbance. Under the circumstances, the nonuniform influences in time and space of roadway size on the propagation of stress waves in surrounding rock can be roughly ignored [22], and then the dynamic loads were regarded as reaching roadway surrounding rocks at the same time and being evenly acted and normally incident on the bearing structure (the red arrow in Figure 1 indicates the incident direction of dynamic loads).

As shown in Figure 1, the ranges of anchored bearing structure, plastic zone excluding anchored bearing structure, and elastic zone are $R_0 \le r \le R_0 + b$, $R_0 + b < r \le R_p$, and $r > R_p$, respectively. In addition, R_0, b, and R_p represent separately the roadway radius, thickness of anchored bearing structure, and radius of plastic zone, which are given by Cheng et al. [23]:

$$\begin{cases} R_{\mathrm{p}} = R_0 \left[\dfrac{(\gamma H + c\cot\varphi)(1-\sin\varphi)}{p + c\cot\varphi} \right]^{\frac{1-\sin\varphi}{2\sin\varphi}} \\ b = l - \dfrac{l + R_0}{R_0} \dfrac{d}{2} \\ b \le R_{\mathrm{p}} - R_0 \le l, \end{cases} \tag{1}$$

where l and d separately represent the length and anchoring interval of the bolt. γ denotes the bulk weight of overlying strata and is generally 25 kN/m^3. H means the buried depth of the roadway. c and ϕ denote the cohesion and internal friction angle of coal-rock mass, respectively.

According to the elastic–plastic mechanics and limit equilibrium theory, the static stresses of plastic zone for semicircular arched roadway under hydrostatic pressure are given by Wang et al. [24]:

$$\begin{cases} \sigma_{r\mathrm{p}} = (p + c\cot\varphi)\left(\dfrac{r}{R_0}\right)^{\frac{2\sin\varphi}{1-\sin\varphi}} \\ -c\cot\varphi\ \sigma_{\theta\mathrm{p}} = (p + c\cot\varphi)\left(\dfrac{1+\sin\varphi}{1-\sin\varphi}\right)\left(\dfrac{r}{R_0}\right)^{\frac{2\sin\varphi}{1-\sin\varphi}} - c\cot\varphi, \end{cases} \tag{2}$$

where $\sigma_{r\mathrm{p}}$ and $\sigma_{\theta\mathrm{p}}$ separately refer to the radial and tangential stress of plastic zone. p is the supporting strength provided by anchor bolts (cables) and meets $p = Q/d^2$, where Q denotes the working resistance of anchor bolts and can be approximated as the pretightening force Q_0. r refers to the distance from any point to roadway center O.

According to the Lame solution in elasticity, the static stresses of elastic zone ($r > R_{\mathrm{p}}$) for semicircular arched roadway under hydrostatic pressure are given by Boresi et al. [25]:

$$\begin{cases} \sigma_{re} = \gamma H\left(1 - \dfrac{R_{\mathrm{p}}^2}{r^2}\right) + q\dfrac{R_{\mathrm{p}}^2}{r^2} \\ \sigma_{\theta\mathrm{e}} = \gamma H\left(1 + \dfrac{R_{\mathrm{p}}^2}{r^2}\right) - q\dfrac{R_{\mathrm{p}}^2}{r^2}, \end{cases} \tag{3}$$

where σ_{re} and $\sigma_{\theta\mathrm{e}}$ refer to the radial and tangential stress of elastic zone, respectively. q is the radial stress at elastic–plastic interface ($r = R_{\mathrm{p}}$) based on Equation (2).

Apart from static stresses during mining, another important factor for the coal burst of roadway is the dynamic disturbance triggered by mine microseisms, which affects surrounding rocks in the form of vibration waves [26]. For the calculation of dynamic failure in the engineering field, it is critical to consider the most dangerous situation of coal burst under peak dynamic stresses. Based on the elastic wave theory, the dynamic stresses on anchored roadway surrounding rocks are given by He [27]:

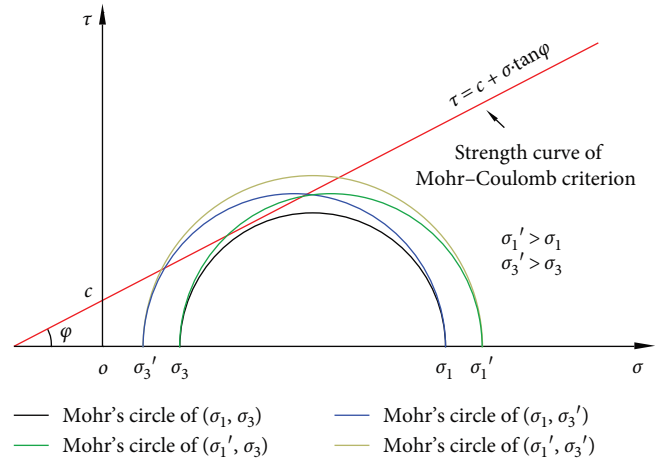

FIGURE 2: Failure modes of coal-rock mass under dynamic disturbance based on Mohr–Coulomb strength criterion.

$$\begin{cases} \sigma_{\mathrm{dP}} = \rho C_{\mathrm{P}} v_0 \cdot L^{-\lambda} \\ \sigma_{\mathrm{dS}} = \rho C_{\mathrm{S}} v_0 \cdot L^{-\lambda}, \end{cases} \tag{4}$$

where σ_{dP} and σ_{dS} separately represent the radial and tangential stress caused by vibration waves propagating to roadway surrounding rocks. ρ is the density of coal-rock mass. C_{P} and C_{S} separately refer to the propagation velocities of P and S waves in coal-rock mass and meet $C_{\mathrm{P}} = 4{,}300$ m/s and $C_{\mathrm{S}} = 2{,}480$ m/s. L refers to the propagation distance of vibration wave, and λ means the attenuation coefficient of vibration waves in coal-rock mass, which is generally 1.526. v_0 is the peak vibration velocity of a particle at the dynamic-loading source, which meets $v_0 = 0.0645 U_{\mathrm{d0}}{}^{0.3566}$, where U_{d0} is the dynamic-loading energy [28].

2.2. Failure Process and Energy Evolution of Elastic Zone. P and S waves are generally generated together at the dynamic-loading source and propagate simultaneously outwards, which means each point on the propagation path of vibration waves experiences compression, tension, and shear in succession so that the normal and tangential stresses with periodically changing magnitude and direction are produced at the point. The above dynamic stresses are superposed with static stresses, which can alter the magnitude and direction of principal stresses. Based on the Mohr–Coulomb strength criterion, the failure of coal-rock mass is likely to occur with the increase in the radius of Mohr's circle. As shown in Figure 2, there are following three possible failure modes: (1) increase of maximum principal stress σ_1; (2) decrease of minimum principal stress σ_3; and (3) increase of σ_1 and decrease of σ_3. The above three failure modes all enlarge the radius of Mohr's circle while do not change the shear strength of materials. Obviously, Mohr's circle in the third failure mode has the largest radius, and correspondingly, the failure range of elastic zone is also the largest. Therefore, the third failure mode is taken as the most concerned failure mode of elastic zone in this research.

The static principal stresses of elastic zone meet $\sigma_1 = \sigma_{\theta\mathrm{e}}$ and $\sigma_3 = \sigma_{re}$ based on Equation (3). Considering that the

most dangerous failure mode is characterized as increase of σ_1 and decrease of σ_3, the principal stresses (σ_1' and σ_3') of elastic zone under dynamic disturbance and the corresponding failure criterion can be expressed as follows:

$$\begin{cases} \sigma_1' = \sigma_{\theta e} + \sigma_{dS} \\ \sigma_3' = \sigma_{re} - \sigma_{dP} \\ \sigma_1' = \dfrac{1+\sin\varphi}{1-\sin\varphi}\sigma_3' + \dfrac{2c\cdot\cos\varphi}{1-\sin\varphi}, \end{cases} \tag{5}$$

where the dynamic stress σ_{dP} and σ_{dS} are calculated by Equation (4), and the corresponding propagation distance L of vibration wave can be calculated approximately as the distance from dynamic loading source to elastic–plastic interface ($r = R_p$) and satisfies $L = L_0 - R_p$.

By simultaneously solving Equations (1)–(5), the maximum radius R_f for the dynamic failure of elastic zone can be obtained, and then the failure region of elastic zone is determined as $R_p \le r \le R_f$.

Afterward, the energy release in elastic zone can be calculated. The elastic energy U_e in failure region of elastic zone can be expressed as follows:

$$U_e = \frac{\overline{\sigma_1}^2 + \overline{\sigma_2}^2 + \overline{\sigma_3}^2 - 2\mu(\overline{\sigma_1}\overline{\sigma_2} + \overline{\sigma_1}\overline{\sigma_3} + \overline{\sigma_2}\overline{\sigma_3})}{2E} \cdot V_f, \tag{6}$$

where V_f denotes the volume of failure region and meets $V_f = 1\cdot\pi\ (R_f^2 - R_p^2)/2$ (the roadway length along axial direction is 1 m for the plane-strain model). E represents the elastic modulus of coal-rock mass. $\overline{\sigma_1}$, $\overline{\sigma_2}$, and $\overline{\sigma_3}$ separately represent the average value of static maximum, intermediate, and minimum principal stresses in failure region of elastic zone.

The above-average values of static principal stresses can be approximated as the static stresses at the middle section ($r = (R_p + R_f)/2$) of failure region ($R_p \le r \le R_f$) based on Equation (3), which are given by the following:

$$\begin{cases} \overline{\sigma_1} = (\sigma_{\theta e})_{r=(R_p+R_f)/2} \\ \overline{\sigma_2} = \mu\left((\sigma_{\theta e})_{r=(R_p+R_f)/2} + (\sigma_{re})_{r=(R_p+R_f)/2}\right), \\ \overline{\sigma_3} = (\sigma_{re})_{r=(R_p+R_f)/2} \end{cases} \tag{7}$$

where μ is Poisson's ratio.

Likewise, the vibration energy U_{de} subjected by the whole failure region of elastic zone ($R_p \le r \le R_f$) is also approximated as the vibration energy at the middle section ($r = (R_p + R_f)/2$) of failure region, which meets $U_{de} = U_{d0}\cdot(L_0 - (R_p + R_f)/2)^{-\lambda}$.

According to the least energy principle of dynamic failure [29], the energy needed for dynamic failure is that for coal-rock damage under uniaxial compression, and then the energy U_{min} consumed during dynamic failure of elastic zone can be expressed as $U_{min} = (\sigma_c^2/2E)\cdot V_f$, where σ_c is the uniaxial compressive strength of coal-rock mass.

Thus, the residual energy U_r of elastic zone after dynamic failure can be expressed as follows:

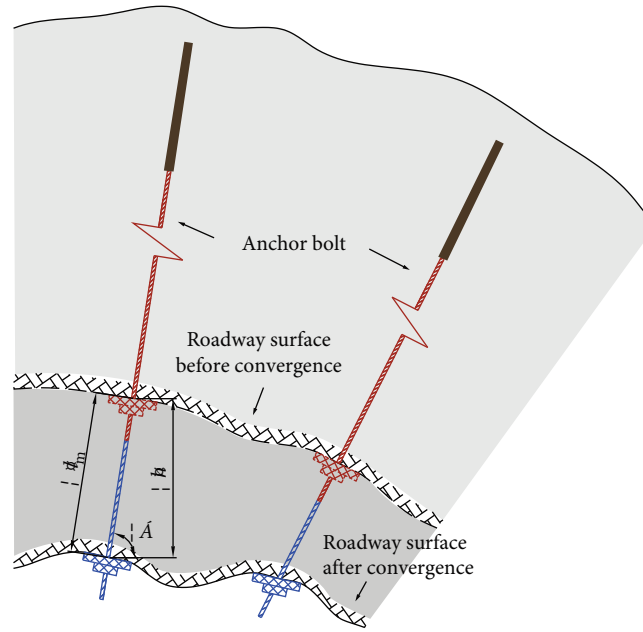

FIGURE 3: Relationship between impact-induced convergence of fractured surrounding rocks and ultimate elongation of bolt.

$$U_r = U_e + U_{de} - U_{min}, \tag{8}$$

when $U_r > 0$, the residual energy U_r mainly propagates outwards as kinetic energy [30], which can impart additional kinetic energy to the anchored bearing structure. In this way, the coal burst of anchored roadway may occur. When $U_r \le 0$, no excessive energy can be released, and then there is no condition of coal burst. Therefore, the existence of residual energy U_r of elastic zone is a prerequisite for the coal burst of anchored roadway surrounding rock.

2.3. Coal Burst Criterion. When $U_r > 0$, the failure region of elastic zone is equivalent to a new source region of dynamic disturbance, whose released kinetic energy attenuates definitely when propagating in the anchored bearing structure. For the convenience of engineering calculation, the kinetic energy at the middle section ($r = R_0 + b/2$) of bearing structure ($R_0 \le r \le R_0 + b$) can be taken as the average kinetic energy of whole structure. Then, the propagation distance L_k of kinetic energy meets $L_k = 1 + R_p - (R_0 + b/2)$, where L_k at the elastic–plastic interface ($r = R_p$) of roadway surrounding rocks equals to 1. In order to analyze the failure situation at each location of roadway surrounding rocks, the anchored bearing structure is divided into 60 microunits with an interval of 3° ($\Delta\alpha$), as shown in Figure 1. In this way, the kinetic energy U_k of bearing structure for any microunit $\Delta\alpha$ is obtained as $U_k = U_r \cdot L_k^{-\lambda_c}/60$, where λ_c is the attenuation coefficient of kinetic energy in bearing structure and is generally 2.131 [31].

It is also necessary to consider the potential energy released from the convergence of fractured surrounding rocks in roadway roof during the impact process [32], as shown in Figure 3, and this part of energy also needs to be resisted by the support system. Thus, the energy U_p imposed

Table 1: Hazard degree classification for coal burst of roadway.

Degree	No hazard	Weak hazard	Moderate hazard	Strong hazard
Hazard index δ	$0 < \delta < 0.25$	$0.25 \le \delta < 0.50$	$0.5 \le \delta < 0.75$	$0.75 \le \delta < 1$

by impact-induced convergence of surrounding rocks on support system in any microunit $\Delta\alpha$ can be expressed as follows:

$$U_p = \rho V_{\Delta a} g \Delta h, \tag{9}$$

where g is the gravitational acceleration. $V_{\Delta\alpha}$ denotes the volume of any microunit $\Delta\alpha$ and meets $V_{\Delta\alpha} = 1 \cdot (\pi\ ((R_0 + b)^2 - R_0{}^2)/2)/60$. Δh denotes the impact-induced convergence (vertical deformation) of fractured surrounding rocks and satisfies $\Delta h = \Delta l_m \cdot \sin\alpha$, where Δl_m is the ultimate elongation of bolt. α represents the included angle between any microunit $\Delta\alpha$ and the positive direction of x-axis and ranges from 0° to 180°.

Obviously, the roadway support system needs to resist and absorb the kinetic energy released from the dynamic failure of elastic zone and potential energy released from convergence of fractured surrounding rocks during the impact process. The ultimate value U_s of absorbed energy of support system in a range of each microunit $\Delta\alpha$ is given by the following:

$$U_s = (\rho_b \cdot U_b \cdot \eta_b + \rho_c \cdot U_c \cdot \eta_c) \cdot S_s, \tag{10}$$

where S_s denotes the roadway surface area corresponding to any microunit $\Delta\alpha$ and meets $S_s = \pi R_0/60 \cdot 1$. where ρ_b and ρ_c refer to anchoring densities of bolts and cables, respectively. U_b represents the absorbed energy for combined supports of a single bolt, steel belts, and metal nets under ultimate deformation. U_c denotes the absorbed energy for a single cable under ultimate deformation. η_b indicates the energy-dissipation coefficient for combined supports of bolt, steel belt, and metal net, while η_c refers to the energy-dissipation coefficient of cable. When η (η_b or η_c) ≤ 1, it reflects the impact-resistance reduction of the actual support system caused by dynamic disturbance, post-peak strain softening, anisotropy of surrounding rocks, inhomogeneity of support strength, and so on. However, $\eta > 1$ means that optimization of existing support parameters and improvement for energy-absorption of support system.

It is because of the anchorage effect of the support system that the active bearing structure of anchored roadway can be formed [23]. Once the support system is damaged, the entire bearing structure will be destructed. When the impact resistance of support is insufficient, the whole anchored roadway will suffer from the coal burst [8, 12]. Energy theory is one of the main theories to reveal the coal burst mechanism [18, 21]. Thus, by taking any microunit $\Delta\alpha$ as the research object, the novel coal burst criterion of anchored roadway surrounding rock can be proposed as follows:

$$U_k + U_p > U_s. \tag{11}$$

In order to quantitatively analyze the coal burst hazard, it is necessary to obtain an evaluation index of hazard based on the coal burst criterion [10, 11]. Thus, the hazard index of coal burst for anchored roadways under dynamic disturbance is proposed as follows:

$$\begin{cases} \delta_\alpha = (U_k + U_p)/U_s \\ \delta = \max\{\delta_\alpha\},\ 0° \le \alpha \le 180° \end{cases}, \tag{12}$$

where δ_α is the hazard index of coal burst for any microunit $\Delta\alpha$. δ is the hazard index of coal burst for the whole anchored bearing structure.

According to Equation (12), the higher the hazard index δ is, the greater the possibility of coal burst for anchored bearing structure. When $\delta > 1$, the bearing structure will be damaged under dynamic disturbance. When $\delta = 1$, the bearing structure is at the critical state of impact failure. When $0 < \delta < 1$, the impact failure will not occur in the bearing structure. According to the conventional grading method for coal burst hazard [9], it can be further graded based on the hazard index δ, as shown in Table 1.

3. Case Analysis

3.1. Site Description. Number 4 coal seam was mined in the 401102 working face of Hujiahe Coal Mine (Shaanxi Province, China), whose average thickness was 22 m. Figure 4 shows the geologic histogram of 401102 working face. The fully mechanized top-coal caving multislicing mining method was adopted in the 401102 working face, with the top slice (12 m) mined first and 10-m thick coal retaining as the bottom slice. The roof was composed of a 0.8-m thick false roof (mudstone), 3.5-m thick immediate roof (medium-grained sandstone), and 11.7-m thick main roof (siltstone). The floor was hard fine sandstone of 5.6-m thick. Table 2 shows the mechanical properties of coal and rock strata in the 401102 working face.

The bursting liability of Number 4 coal seam is presented in Table 3, where D_T, W_{ET}, and K_E represent the duration of dynamic fracture, elastic strain energy index, and bursting energy index, respectively. Moreover, the bending energy index U_{WQS} of the main roof (siltstone) was 19.75 kJ (15 kJ $< U_{WQS} \le$ 120 kJ), whose bursting liability belonged to Class II. According to the Chinese national standard GB/T 25217.1-2010 and GB/T 25217.2-2010, Number 4 coal seam and its main roof have strong and weak bursting liabilities, respectively.

The air-return roadway in 401102 working face was arranged along the bottom of the top slice, whose buried depth H was 600 m. The semicircular arched section was

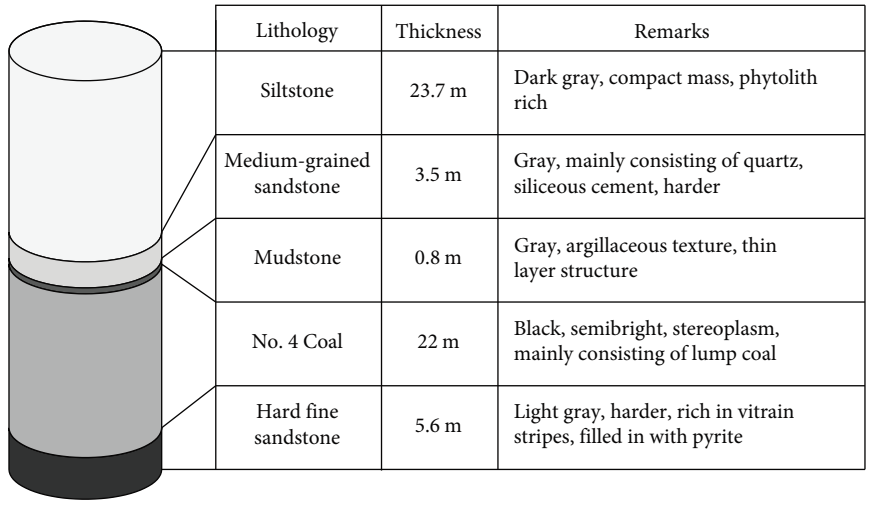

Figure 4: Geologic histogram of 401102 working face.

Table 2: Mechanical properties of coal and rock strata in 401102 working face.

Lithology	Density (kg/m^3)	Elastic modulus (GPa)	Uniaxial compressive strength (MPa)	Poisson's ratio	Cohesion (MPa)	Internal friction angle (°)
Siltstone	2,370	8.7	26.1	0.24	4.2	35
Medium-grained sandstone	2,450	6.3	23.2	0.25	3.8	33
Mudstone	2,260	5.4	18.6	0.28	3.3	32
Number 4 coal seam	1,400	2.0	12.5	0.35	2.0	30
Hard fine sandstone	2,530	10.5	28.4	0.22	4.7	38

Table 3: Bursting liability of Number 4 coal seam.

Slice of Number 4 coal seam	Index				Determination results	
	D_T (ms)	W_{ET}	K_E	σ_c (MPa)	Class	Bursting liability
Top slice	39.80	6.49	7.73	12.57	III	Strong
Bottom slice	34.40	5.45	12.57	12.45	III	Strong

adopted in air-return roadway, with a net height of 4 m and net width of 5 m, which means the roadway radius R_0 in theoretical model is about 2.5 m. The combined supports of anchor bolts, anchor cables, metal nets, and steel belts were used in air-return roadway. Figure 5 shows the layout and supporting scheme of air-return roadway. The high-strength threaded steel bolt (MSGLW500) was used, with a diameter of 20 mm, length l of 2,400 mm, anchoring length of 450 mm, pretightening force Q_0 of 60 kN, ultimate elongation Δl_m of 0.292 m, and anchoring interval d of 0.8 m. The diameter of anchor cable was 17.8 mm, with a length of 6,300 mm and an ultimate elongation of 0.207 m. For the support density, 1.56 bolts (ρ_b) and 0.18 anchor cables (ρ_c) were arranged per square meter. By referring to similar support conditions [33], the absorbed energy U_b for combined supports of a single bolt, steel belts, and metal nets under ultimate deformation was taken as 20 kJ, and the absorbed energy U_c for a single cable under ultimate deformation was set as 30 kJ. The energy-dissipation coefficient η_b and η_c were both set as 0.7. The gravitational acceleration g was 10 m/s^2.

3.2. Distribution of Coal Burst Hazard. The air-return roadway of 401102 working face was significantly affected by dynamic disturbance during coal mining, and microseismic events mainly occurred inside the main roof. Based on the above geological and mining conditions, the dynamic-loading energy U_{d0} of 5×10^5 J inside the main roof was taken as the example, whose distance L_0 from the roadway center was 20 m. Then, the hazard indexes δ_α of coal burst and energy U_p imposed by impact-induced convergence of surrounding rocks on the support system in different components of roadway were obtained using the calculation flowchart in Section 2.

Figure 6 shows distributions of δ_α and U_p, only changing the included angle α between microunit $\Delta\alpha$ in bearing structure and positive direction of x axis. It is found that both δ_α

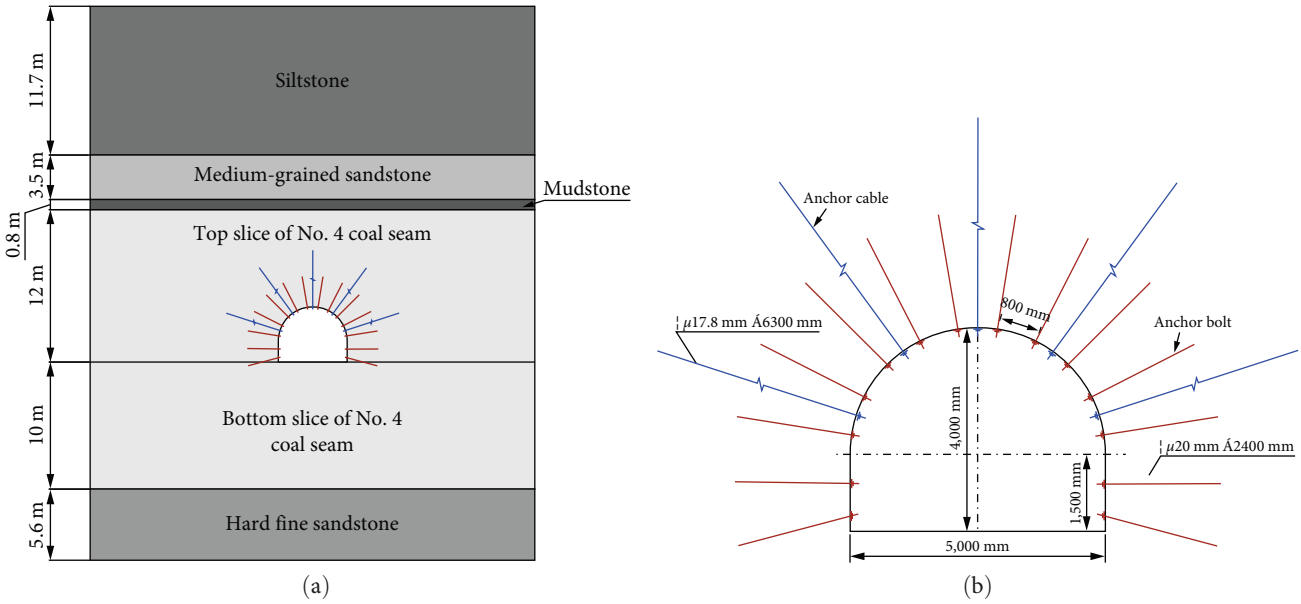

FIGURE 5: Layout and supporting scheme of air-return roadway: (a) layout; (b) supporting scheme.

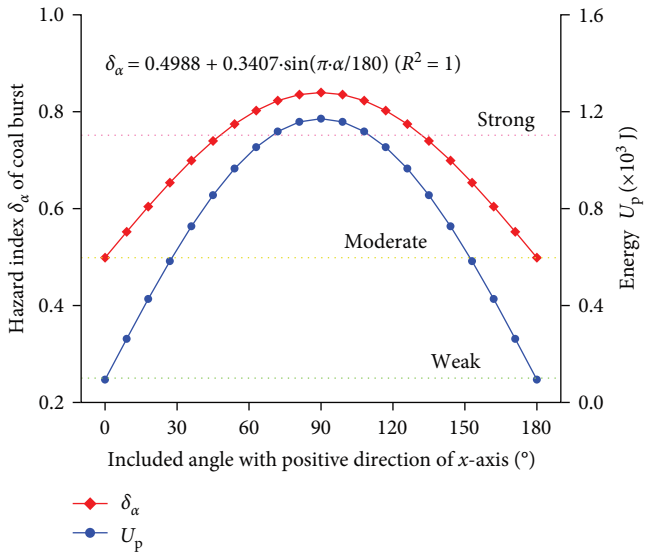

FIGURE 6: Distributions for hazard index δ_α of coal burst and energy U_p of microunits at different components of roadway.

and U_p are distributed in a symmetric manner, being large in the middle while small in two sides. The corresponding relationship between δ_α and α is expressed as $\delta_\alpha = 0.4988 + 0.3407\cdot\sin(\pi\cdot\alpha/180)$ ($R^2 = 1$). The maximum values of δ_α and U_p ($\delta_{\alpha\max} = 0.84$ and $U_{p\text{-}\max} = 1.14 \times 10^3$ J) are both found at the position of $\alpha = 90°$ (the middle part of roadway roof). However, the minimum values ($\delta_{\alpha\min} = 0.50$ and $U_{p\text{-}\min} = 0$) are observed at the positions of $\alpha = 0°$ (left sidewall) and $\alpha = 180°$ (right sidewall). The above results indicate that the closer to the roadway roof is, the larger the potential energy released from impact-induced deformation of anchored surrounding rocks and the greater the total impact energy resisted by the support system, which causes a higher hazard index δ_α of coal burst. Therefore, the roadway roof is more prone to impact failure than two sidewalls under the same support conditions and thus is the critical area for coal burst prevention.

3.3. Influences of Main Controlling Factors. Influences of main controlling factors on the hazard index of coal burst were revealed based on four characteristic parameters of impact failure, including the residual energy U_r of elastic zone after dynamic failure, kinetic energy U_k of bearing structure, failure range ΔR_f ($\Delta R_f = R_f - R_p$) of elastic zone and range ΔR_p ($\Delta R_p = R_p - R_0$) of plastic zone.

3.3.1. Buried Depth of Roadway. Figure 7 shows the influence for buried depth H of roadway on coal burst hazard. It is found that the hazard index δ of coal burst and original rock stress σ_0 ($\sigma_0 = \gamma H$) [34] both have positive correlations with H. The fitting relationship between δ and H is expressed as $\delta = 0.4345 \cdot H^{0.3664}$ ($R^2 = 0.9978$). In addition, the stress level of surrounding rocks grows with the increasing buried depth, so that the same dynamic load exerts slightly decreased influences on the stress state of elastic zone, and the failure range ΔR_f of elastic zone induced by dynamic loading also shrinks correspondingly. While the influence of an increase in stress level on elastic energy U_e in failure region of elastic zone is significantly higher than that of a decrease in failure range ΔR_f of elastic zone, and thus the residual energy U_r in elastic zone after dynamic failure rises prominently. Besides, the range ΔR_p of plastic zone is enlarged with the buried depth according to Equation (1). The above results lead to the slight growth for kinetic energy U_k of bearing structure, which causes the slow enlargement of δ based on Equation (12).

3.3.2. Cohesion of Surrounding Rock. Cohesion is the critical parameter characterizing the mechanical property of surrounding rock, which can indirectly reflect the strength of surrounding rock [24]. Figure 8 shows the influence for

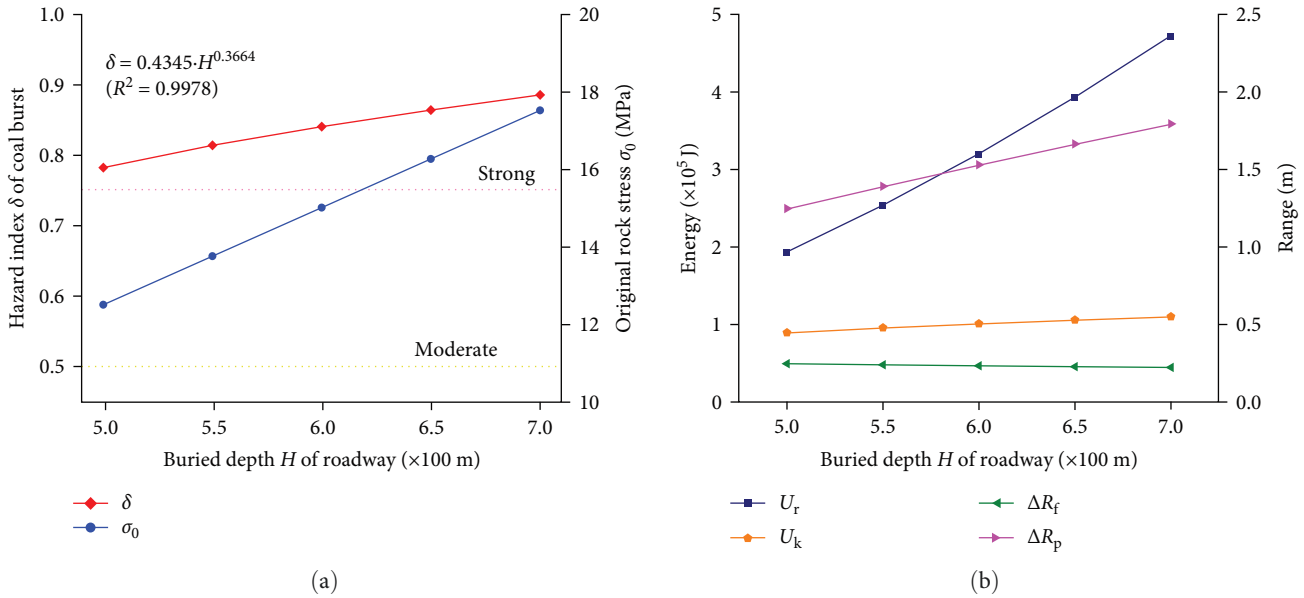

FIGURE 7: Influence for buried depth H of roadway on coal burst hazard: (a) δ and σ_0; (b) U_r, U_k, ΔR_f, and ΔR_p.

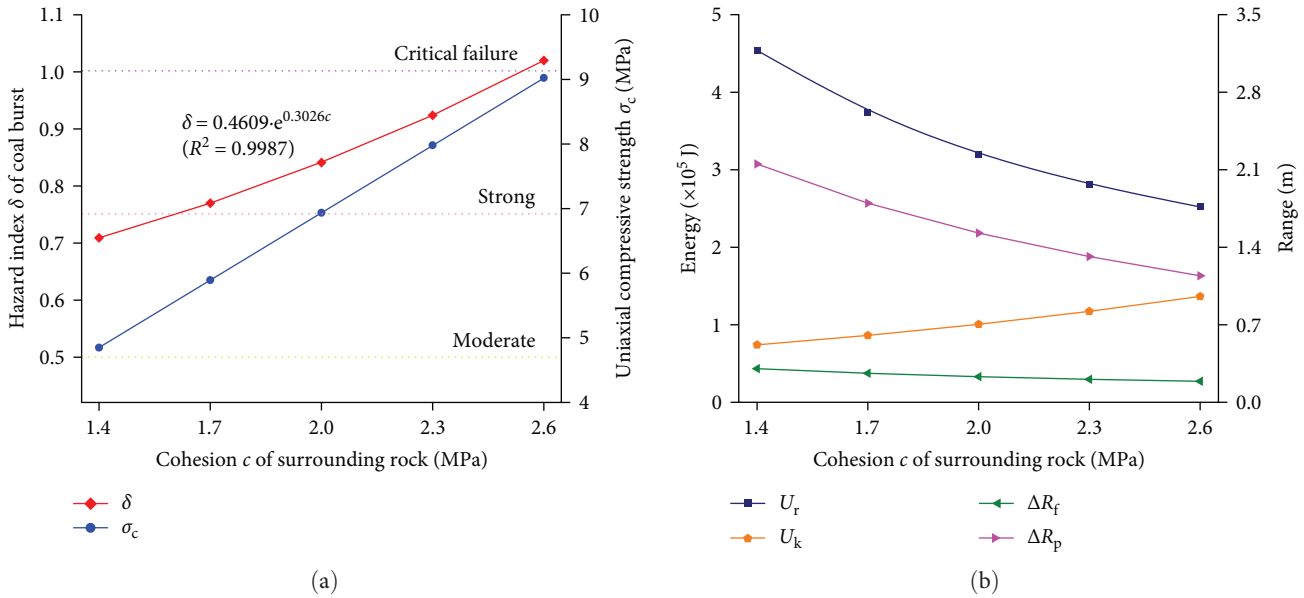

FIGURE 8: Influence for cohesion c of surrounding rock on coal burst hazard: (a) δ and σ_c; (b) U_r, U_k, ΔR_f, and ΔR_p.

cohesion c of surrounding rock on coal burst hazard. It is found that the hazard index δ of coal burst and uniaxial compressive strength σ_c ($\sigma_c = 2c \cdot \cos\varphi/(1-\sin\varphi)$) both have positive correlations with cohesion c of surrounding rock, and the fitting relationship between δ and c is expressed as $\delta = 0.4609 \cdot e^{0.3026c}$ ($R^2 = 0.9987$). Besides, the strength of surrounding rocks enlarges with the increasing cohesion, so the failure range ΔR_f of elastic zone induced by the same dynamic load decreases, and the residual energy U_r in elastic zone after dynamic failure also reduces, whereas the increase of cohesion c also significantly shrinks the range ΔR_p of plastic zone, which weakens the dissipation of U_r through the bearing structure. Thus, the kinetic energy U_k of bearing structure increases correspondingly, which eventually leads to the rise in δ. It is stipulated in the Chinese national standard GB/T 25217.2-2010 that the larger the σ_c, the higher the coal burst tendency and the easier the coal burst to occur, which well verifies the above analysis results regarding the correlation between cohesion (uniaxial compressive strength) and hazard index of coal burst for anchored roadway.

3.3.3. Dynamic-Loading Energy. The breaking of thick-hard rock strata can trigger high-energy dynamic disturbances, which act on roadway surrounding rocks [30]. Thus, the dynamic-loading energy can reflect the disturbance effect

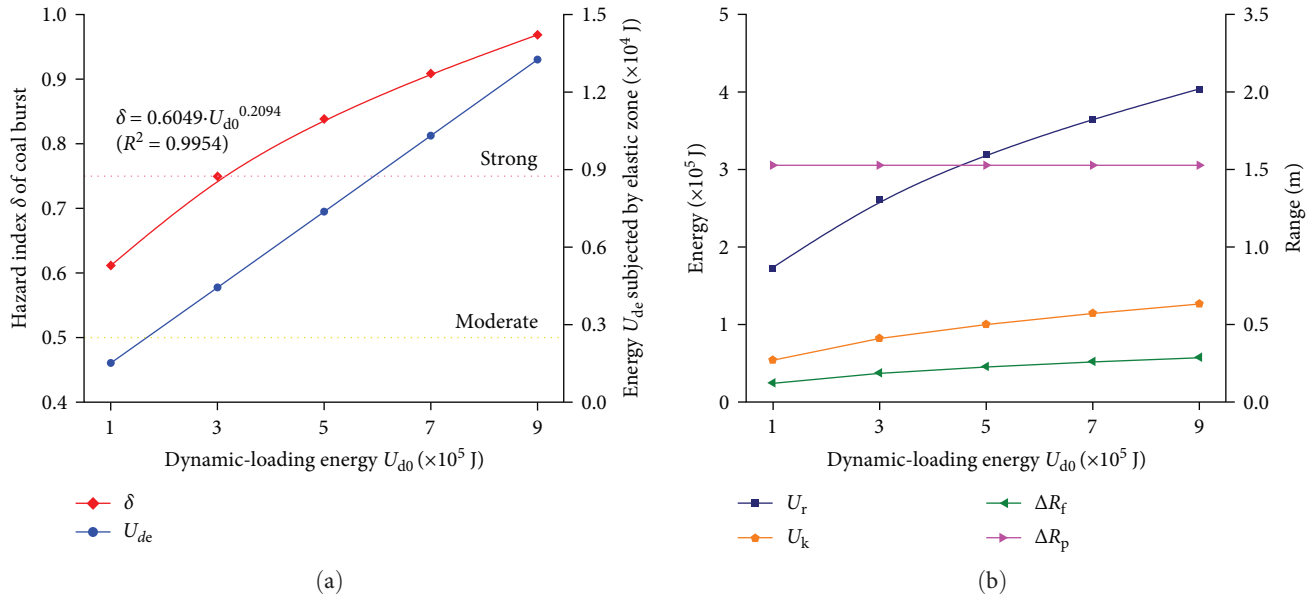

FIGURE 9: Influence for dynamic-loading energy on coal burst hazard: (a) δ and U_{de}; (b) U_r, U_k, ΔR_f, and ΔR_p.

of external factors on anchored roadway. Figure 9 shows the influence for dynamic-loading energy on coal burst hazard. It is found that the hazard index δ of coal burst and vibration energy U_{de} ($U_{de} = U_{d0} \cdot (L_0 - (R_p + R_f)/2)^{-\lambda}$) subjected by failure region of elastic zone both have positive correlations with dynamic-loading energy U_{d0}, and the fitting relationship between δ and U_{d0} is expressed as $\delta = 0.6049 \cdot U_{d0}^{0.2094}$ ($R^2 = 0.9954$). Moreover, the dynamic stress σ_d enlarges with the increase of U_{d0} according to Equation (4), so that the failure range ΔR_f of elastic zone caused by dynamic loading enlarges as well, and correspondingly the residual energy U_r in elastic zone after dynamic failure also rises. Moreover, the range ΔR_p of plastic zone remains unchanged, so the dissipation of U_r through bearing structure also does not change. Thus, the kinetic energy U_k of bearing structure increases, which finally induces the rise in δ.

3.3.4. Energy-Absorption Capability of Support. Figure 10 shows the influence for the energy-absorption capability of support on coal burst hazard. It is found that hazard index δ of coal burst is negatively correlated with energy-dissipation coefficient η, meeting $\delta = 0.5618 \cdot \eta^{-1}$ ($R^2 = 1$), while absorbed energy u_s ($u_s = (\rho_b \cdot U_b + \rho_c \cdot U_c) \cdot \eta$) of roadway support system per unit surface area is positively correlated with η. The above results indicate that the coal burst hazard of anchored roadway can be effectively reduced by improving the energy-absorption capacity of the support system, such as using anchor bolts with constant resistance and large deformation [35], energy-absorbing anchor bolts, cables, and trays [36]. In addition, it is worth noting that relevant characteristic parameters of impact failure (U_r, U_k, ΔR_f, and ΔR_p) are all not affected by changes in the energy-dissipation coefficient of the support system. The energy-dissipation coefficient η is abstract for engineering practice, and then the in-situ energy-absorption capacity of support can be indirectly characterized by monitoring the change of support resistance. There

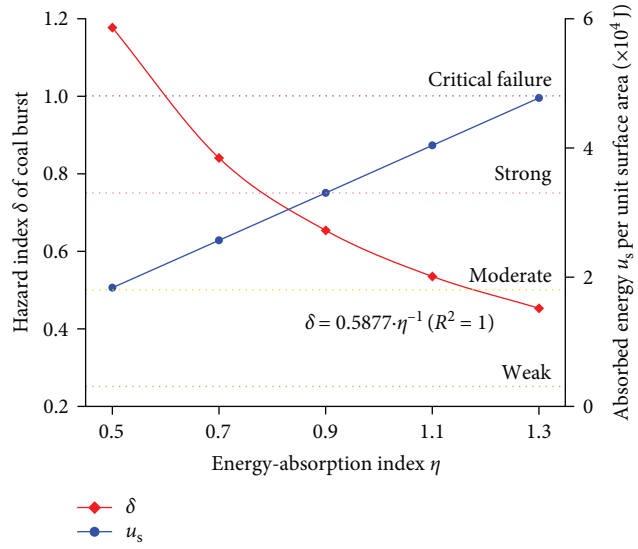

FIGURE 10: Influence for energy-absorption capability of support on coal burst hazard.

are many factors affecting the energy-absorption capacity, including dynamic disturbance, post-peak strain softening of surrounding rocks, heterogeneity of surrounding rocks, inhomogeneity of support strength, etc. When the energy-absorption effect of overall support is reduced due to the above influential factors, the risk of coal burst will correspondingly increase.

3.4. Verification in Practice. A coal burst disaster occurred in the air-return roadway of 401102 working face in Hujiahe Coal Mine at 19:56 PM on October 4, 2014. The dynamic loading source ($U_{d0} = 1.9 \times 10^6$ J) was located inside the main roof (siltstone) and had a distance L_0 of 22.4 m with the roadway center. This dynamic instability triggered large

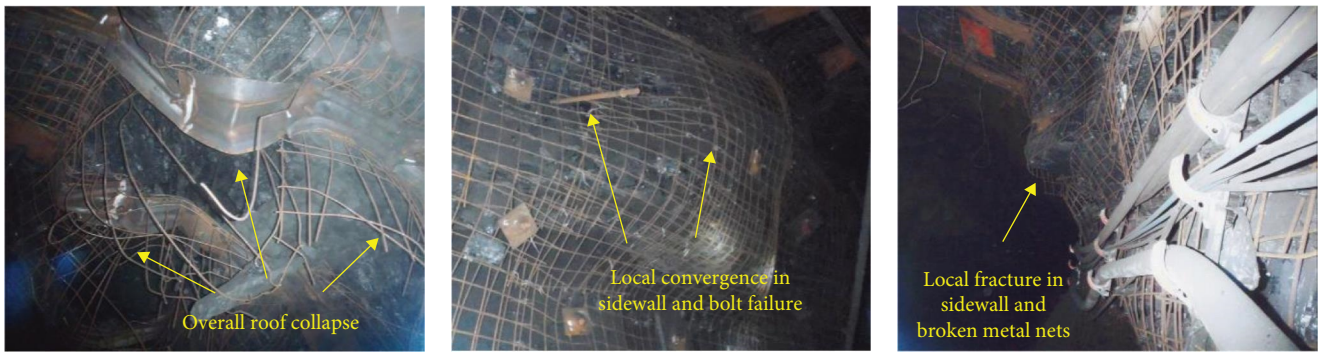

Figure 11: Dynamic failure of air-return roadway in 401102 working face: (a) roof; (b) left sidewall; (c) right sidewall.

areas of caving, mesh cracking, and significant subsidence of roadway roofs in the region being 24–36 m from the working face, as well as obvious deformation and spalling in sidewalls near the arch corner, as shown in Figure 11. The roadway roof was damaged most significantly (subsidence of 400–600 mm), followed successively by the left sidewall (convergence of 300–400 mm) and right sidewall (convergence of 100–250 mm). This indirectly expounds that the roadway roof was at higher impact risk than sidewalls, verifying distributions of the hazard index δ_α of coal burst at different components of roadway. In addition, the left sidewall was more seriously damaged than the right sidewall, which also indicates the difference in energy-absorption capacity of support in actual roadway surrounding rocks due to many causes.

Because the air-return roadway had experienced lots of dynamic disturbances before this coal burst, which deteriorated the strength of anchored surrounding rocks and, to some extent, reduced the impact-resistance of the support system, the energy-dissipation coefficient η (η_b and η_c) for the whole roadway support can be set as 0.65. Based on the geological and mining conditions of air-return roadway as well as microseismic parameters of this coal burst, the hazard index δ_α of coal burst at different components of the roadway is obtained according to the calculation process in Section 2 and meets $0.73 \le \delta_\alpha \le 1.10$, and then the hazard index δ for whole bearing structure satisfies $\delta = 1.10 > 1$, reaching the occurrence condition of coal burst. The calculation results are generally consistent with the on-site destruction of coal bursts, verifying the reasonability of the novel coal burst criterion. Further calculation shows that the components of the roadway meeting $\delta_\alpha > 1$ are in the range of $48^\circ \le \alpha \le 132^\circ$, indicating that large areas of surrounding rocks near the roadway roof are subjected to impact failure, which is basically consistent with the overall collapse of roadway roof (Figure 11(a)). While the components of roadway meeting $0.73 \le \delta_\alpha \le 1$ are near to the sidewalls, where the hazard index δ_α of coal burst is calculated based on the average level ($\eta = 0.65$) of energy-dissipation coefficient for whole support. Thus, there are still some surrounding rocks with $\eta < 0.65$ and $\delta_\alpha > 1$ due to the anisotropy of surrounding rocks and inhomogeneity of support strength. These regions are characterized by partial impact failures of roadway supporting, which is basically consistent with on-site local deformations and support failures in two sidewalls (Figures 11(b) and 11(c)).

Figure 12 shows distributions of average anchoring forces and their losses for anchor bolts measured at three measuring points in the coal burst region after its occurrence on October 4, 2014. According to regulations in MT146.1-2010 [37], the anchoring force of bolts should not be lower than 1.2 times of yield strength of bolts. Thus, the design anchoring force should not be lower than 190 kN for the anchor bolt with a yield strength of 500 MPa. Inside the roadway roof (Figure 12(a)), the anchoring forces after coal burst at the vault (104 kN), left haunch (112 kN), and right haunch (123 kN) are listed in an ascending order, which indicates that the closer to the middle part of roadway roof, the more significant the impact failure of surrounding rocks and the greater the loss of anchoring force, which is consistent with the distribution for hazard index δ_α of coal burst. As shown in Figure 12(b), the anchoring forces after coal burst at the roof (113 kN), left sidewall (129 kN), and right sidewall (141 kN) are listed in an increasing order, all significantly lower than the design anchoring force 190 kN. Besides, the ratios of anchoring force after coal burst to design anchoring force at the roof (0.60), left sidewall (0.68), and right sidewall (0.74) are ranked in an ascending order. The above results further verify that the degree of impact failure decreases following the order of the roof, left sidewall, and right sidewall and indicates that the coal burst of roadway can induce the loss of anchoring force and renders the support system to gradually lose impact resistance.

Another coal burst disaster occurred in the air-return roadway of 401102 working face on November 27, 2014. The dynamic loading source was also located inside the main roof with microseismic energy of 1.1×10^6 J. The testing device of surrounding rock strength was used to conduct in-situ strength tests on coal-rock masses within a 10 m range of surrounding rocks before and after coal burst [20]. Figure 13 shows distributions of surrounding rock strengths measured at one measuring point in the coal burst region on November 27, 2014. It is found that the average values of surrounding rock strengths in the roadway roof and

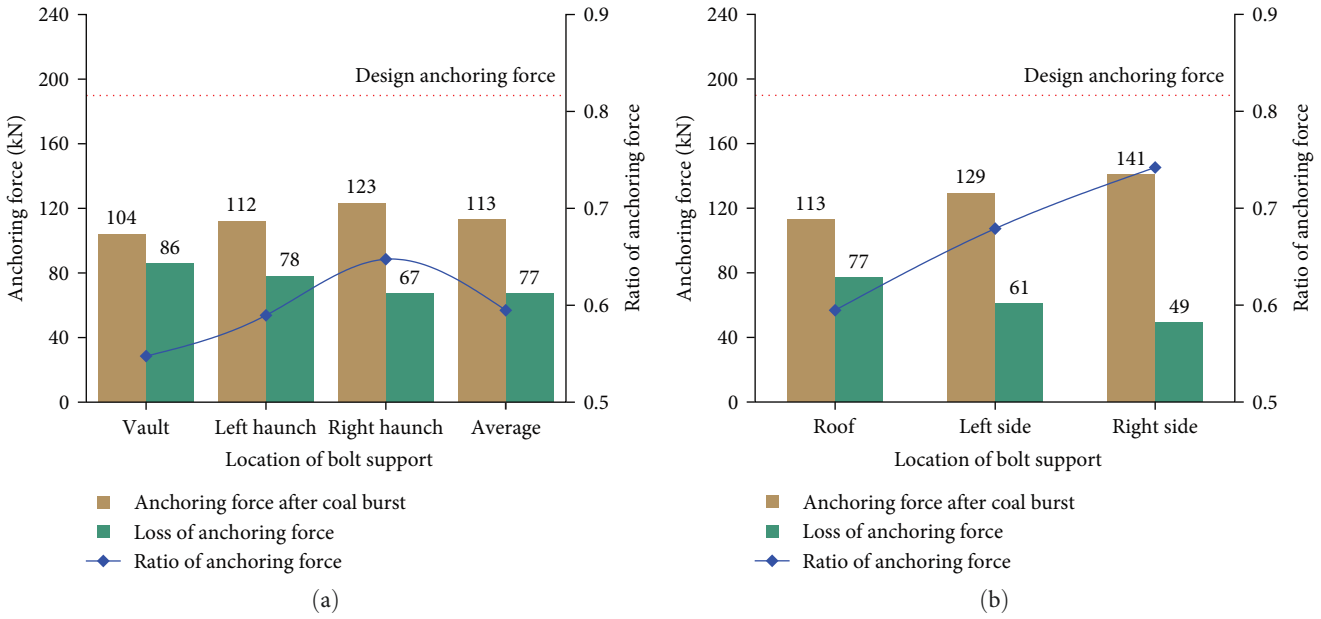

Figure 12: Distributions of average anchoring forces and their losses after coal burst: (a) roadway roof; (b) whole roadway.

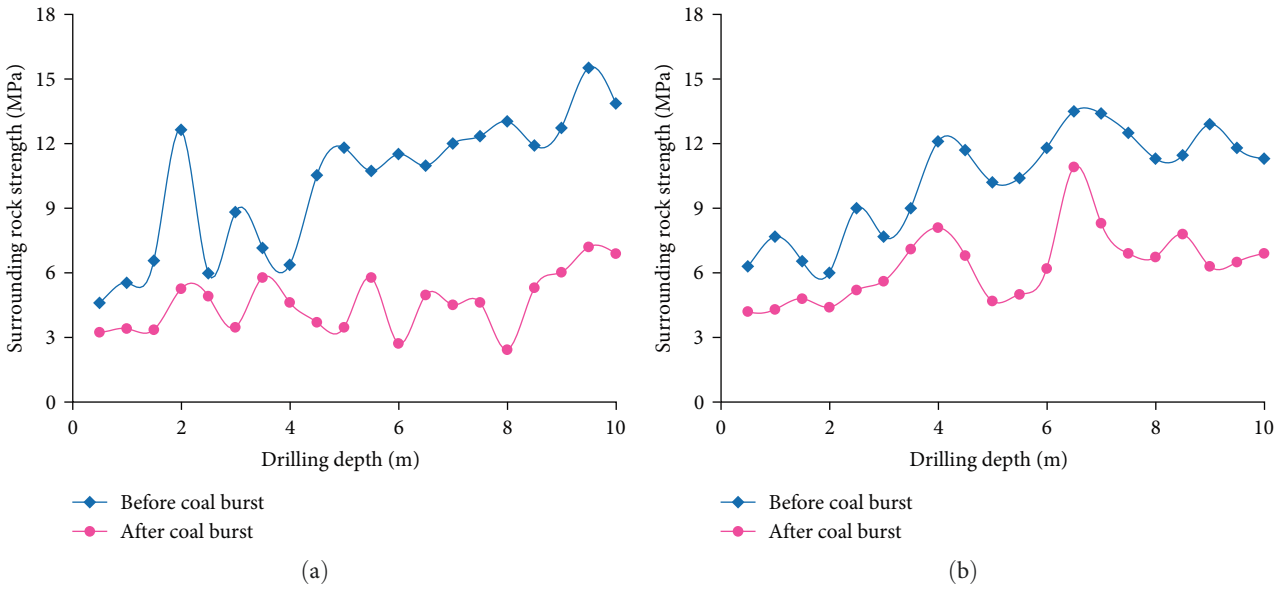

Figure 13: Surrounding rock strength of air-return roadway in 401102 working face before and after coal burst: (a) roadway roof; (b) roadway sidewall.

sidewall after coal burst are 4.6 and 6.3 MPa, respectively. However, the average values of surrounding rock strengths in the roadway roof and sidewall measured during the excavation (before coal burst) are 10.2 and 10.4 MPa, respectively. This coal burst caused a 55.2% decrease in the surrounding rock strength of roadway roof while a 38.6% decrease in that of roadway sidewall. Obviously, the decrease in the surrounding rock strength of roadway roof is more significant than that of roadway sidewall, indicating that the impact failure of roadway roof under dynamic disturbance is more severe than that of roadway sidewall. The above results once again verify the correctness of the novel criterion and hazard index of coal burst.

4. Application in Coal Burst Prevention and Control

The novel criterion and hazard index of coal bursts can be applied to provide some useful references for coal burst prevention and control. First, it can be determined whether the on-site roadway will experience the coal burst based on this criterion. Besides, this novel hazard index can be used to

evaluate the hazard degree and divide the hazard zone of coal burst, which can provide a theoretical basis for optimizing the mining design of anti-impact. Furthermore, according to the above evolution laws of hazard index with main controlling factors, targeted prevention and control measures of coal burst can be formulated, whose specific parameters can be obtained based on safety requirements. Specific references of coal burst prevention and control are as follows:

(1) For areas with a strong hazard of coal burst, their anti-impact capabilities can be improved effectively by strengthening support parameters [12], using high-strength prestressed yielding bolts [38], constant resistance large deformation bolts, and energy-absorbing coupling supports [14]. It is also important to strengthen the monitoring of roadway support resistance and surrounding rock deformation to timely find the support failure area and implement support reinforcement [4].

(2) The hazard degree of coal burst increases gradually after entering deep mining, while the buried depth of roadway cannot be changed. Thus, it is necessary to take measures in advance from reducing static and dynamic loads of surrounding rocks and improving supporting performances [2].

(3) In order to reduce the strength and bursting liability of coal-rock masses and transfer high static stresses to deep surrounding rocks, the pressure-relief measures should be reasonably carried out outside the roadway support structure, such as pressure-relief blasting [39], large diameter pressure-relief drilling, water-infusion softening, etc.

(4) Reducing the dynamic-loading energy is the main method for controlling dynamic disturbances. The presplitting blasting and directional hydraulic fracturing in the roof [40] can be adopted for dynamic loading caused by fracture of overlying strata.

(5) For the roadway after coal burst, it is necessary to determine the main reasons and controlling factors for coal burst. The deformed roadway needs to be repaired to the design size, and then the bolting support should be reinstalled according to the above reference (1). In addition, the existing prevention and control measures also need to be redesigned and re-executed according to safety requirements.

5. Conclusions

In this study, coal burst occurrence of anchored roadway under dynamic disturbance was investigated. A mechanical analysis model for the bearing structure of roadway surrounding rock was built to propose a novel coal burst criterion. Moreover, the study discussed the distribution of the hazard index of coal burst and the influences of main controlling factors based on case analysis and then clarified the application of novel criterion and hazard index in coal burst prevention and control. The main conclusions are as follows:

(1) The existence of residual energy U_r of elastic zone is a prerequisite for coal burst of anchored roadway surrounding rock. The roadway support with ultimate value U_s of absorbed energy needs to resist and absorb the kinetic energy U_k released from the dynamic failure of elastic zone and the energy U_p imposed by impact-induced convergence of surrounding rocks on the support system, and then the novel coal burst criterion can be proposed as $U_k + U_p > U_s$.

(2) Under the same support conditions, the roadway roof is more prone to dynamic failure, which is a critical area for coal burst prevention. Quantitative influences of main controlling factors on coal burst hazard can be revealed based on four characteristic parameters of impact failure, including U_r, U_k, ΔR_f, and ΔR_p.

(3) The novel criterion and hazard index of coal burst can be applied to provide some useful references for coal burst prevention and control, which contain improvements for the anti-impact capability of support, pressure-relief in surrounding rocks, reduction of dynamic-loading energy, and roadway restoration after coal burst.

Nomenclature

L_0: Distance from dynamic disturbance to roadway center (m)
L: Propagation distance of vibration wave (m)
σ_{dP}, σ_{Ds}: Radial and tangential stress caused by vibration waves propagating to roadway surrounding rocks (MPa)
R_0: Roadway radius (m)
R_p: Radius of plastic zone (m)
b: Thickness of anchored bearing structure (m)
l: Bolt length (m)
d: Anchoring interval of bolt (m)
γ: Bulk weight of overlying strata (kN/m^3)
H: Buried depth of roadway (m)
c: Cohesion of coal-rock mass (MPa)
φ: Internal friction angle of coal-rock mass (°)
σ_{rp}, $\sigma_{\theta p}$: Radial and tangential stress of plastic zone (MPa)
p: Supporting strength (MPa)
Q, Q_0: Working resistance and pre-tightening force of anchor bolt (kN)
q: Radial stress at elastic–plastic interface (MPa)
σ_{re}, $\sigma_{\theta e}$: Radial and tangential stress of elastic zone (MPa)
ρ: Density of coal-rock mass (kg/m^3)
C_P, C_S: Propagation velocities of P and S waves in coal-rock mass (m/s)
v_0: Peak vibration velocity of particle at dynamic-loading source (m/s)
λ: Attenuation coefficient of vibration waves in coal-rock mass

U_{d0}: Dynamic-loading energy (J)
σ_1, σ_3: Static maximum and minimum principal stress (MPa)
σ_1', σ_3': Maximum and minimum principal stresses under dynamic disturbance (MPa)
R_f: Dynamic failure radius of elastic zone (m)
$\bar{\sigma}_1$, $\bar{\sigma}_2$, $\bar{\sigma}_3$: Average values of static maximum, intermediate, and minimum principal stresses (MPa)
μ: Poisson's ratio
E: Elastic modulus of coal-rock mass (GPa)
U_e: Elastic energy in failure region of elastic zone (J)
V_f: Volume of failure region (m^3)
U_{de}: Vibration energy subjected by the whole failure region of elastic zone (J)
σ_c: Uniaxial compressive strength of coal-rock mass (MPa)
U_{min}: Energy consumed during dynamic failure of elastic zone (J)
U_r: Residual energy of elastic zone after dynamic failure (J)
u_s: Ultimate value of absorbed energy for roadway support system per unit surface area before impact failure (J/m^2)
ρ_b, ρ_c: Anchoring densities of bolts and cables (number/m^2)
U_b: Absorbed energy for combined supports of a single bolt, steel belts, and metal nets under ultimate deformation (J)
U_c: Absorbed energy for a single cable under ultimate deformation (J)
η: Energy-dissipation coefficient of support
η_b: Energy-dissipation coefficient for combined supports of bolt, steel belt, and metal net
η_c: Energy-dissipation coefficient of cable
U_s: Ultimate value of absorbed energy of support system in range of any microunit (J)
S_s: Roadway surface area corresponding to any microunit (m^2)
L_k: Propagation distance of kinetic energy in bearing structure (m)
U_k: Kinetic energy of bearing structure for any microunit (J)
λ_c: Attenuation coefficient of kinetic energy in bearing structure
U_p: Energy imposed by impact-induced convergence of surrounding rocks on support system in any microunit (J)
g: Gravitational acceleration (m/s^2)
$V_{\Delta\alpha}$: Volume of any microunit (m^3)
Δh: Impact-induced convergence of fractured surrounding rocks (m)
Δl_m: Ultimate elongation of bolt (m)
α: Included angle between any microunit and positive direction of x-axis (°)
δ_α: Hazard index of coal burst for any microunit
δ: Hazard index of coal burst for whole anchored bearing structure
D_T: Duration of dynamic fracture (ms)
W_{ET}: Elastic strain energy index
K_E: Bursting energy index
U_{WQS}: Bending energy index
ΔR_f: Failure range of elastic zone (m)
ΔR_p: Range of plastic zone (m)
σ_0: Original rock stress (MPa).

Data Availability

The data supporting the results can be obtained by emailing a request to author Zheng-yi Wang.

Conflicts of Interest

The authors declare no competing interests.

Acknowledgments

This work was supported by the Natural Science Foundation of the Jiangsu Higher Education Institutions of China (no. 20KJB440001), whose director is Zheng-yi Wang.

References

[1] M. He, F. Ren, and D. Liu, "Rockburst mechanism research and its control," *International Journal of Mining Science and Technology*, vol. 28, no. 5, pp. 829–837, 2018.
[2] Z. Lubosik, S. Rajwa, A. Walentek, W. Masny, A. Wrana, and V. M. Pasculescu, "The role of powered support in ensuring the proper longwall working cross-section area in rockburst-prone seams," *MATEC Web of Conferences*, vol. 305, no. 5, Article ID 00081, 2020.
[3] P. Litwa and G. Merta, "Application of selected analytical and empirical methods to determine the causes of a rock burst incident recorded in a Polish mine," *Journal of Mining Science*, vol. 57, no. 6, pp. 911–921, 2021.
[4] V. I. German and V. A. Mansurov, "Induced seismicity monitoring and procedure of rock-burst focus localization," *Journal of Mining Science*, vol. 38, no. 4, pp. 336–343, 2002.
[5] C. Mark, "Coal bursts in the deep longwall mines of the United States," *International Journal of Coal Science & Technology*, vol. 3, no. 1, pp. 1–9, 2016.
[6] A. Keneti and B.-A. Sainsbury, "Review of published rockburst events and their contributing factors," *Engineering Geology*, vol. 246, pp. 361–373, 2018.
[7] T. Hauquin, Y. Gunzburger, and O. Deck, "Predicting pillar burst by an explicit modelling of kinetic energy," *International Journal of Rock Mechanics and Mining Sciences*, vol. 107, pp. 159–171, 2018.
[8] G.-F. Wang, S.-Y. Gong, L.-M. Dou, W. Cai, F. Jin, and C.-J. Fan, "Behaviour and bursting failure of roadways based on a pendulum impact test facility," *Tunnelling and Underground Space Technology*, vol. 92, Article ID 103042, 2019.
[9] L. Xu, K. Lu, Y. Pan, and Z. Qin, "Study on rock burst characteristics of coal mine roadway in China," *Energy Sources, Part A: Recovery, Utilization, and Environmental Effects*, vol. 44, no. 2, pp. 3016–3035, 2022.
[10] R. Shukla, M. Khandelwal, and P. K. Kankar, "Prediction and assessment of rock burst using various meta-heuristic approaches," *Mining Metallurgy & Exploration*, vol. 38, no. 3, pp. 1375–1381, 2021.

[11] C. Zhang, I. Canbulat, F. Tahmasebinia, and B. Hebblewhite, "Assessment of energy release mechanisms contributing to coal burst," *International Journal of Mining Science and Technology*, vol. 27, no. 1, pp. 43–47, 2017.

[12] K. Skrzypkowski, W. Korzeniowski, K. Zagórski, and A. Zagórska, "Adjustment of the yielding system of mechanical rock bolts for room and pillar mining method in stratified rock mass," *Energies*, vol. 13, no. 8, Article ID 2082, 2020.

[13] A. Mottahedi and M. Ataei, "Fuzzy fault tree analysis for coal burst occurrence probability in underground coal mining," *Tunnelling and Underground Space Technology*, vol. 83, pp. 165–174, 2019.

[14] F. Tahmasebinia, C. Zhang, C. Wei, I. Canbulat, S. Saydam, and S. Sepasgozar, "A new concept to design combined support under dynamic loading using numerical modelling," *Tunnelling and Underground Space Technology*, vol. 117, Article ID 104132, 2021.

[15] Z.-Y. Wang, L.-M. Dou, and G.-F. Wang, "Failure mechanism of anchored bolt supporting structure of circular roadway under dynamic load," *Chinese Journal of Geotechnical Engineering*, vol. 37, no. 10, pp. 1901–1909, 2015.

[16] D. Song, X. He, E. Wang, Z. Li, M. Wei, and H. Mu, "A dynamic ejection coal burst model for coalmine roadway collapse," *International Journal of Mining Science and Technology*, vol. 29, no. 4, pp. 557–564, 2019.

[17] M. Zhang and F. Jiang, "Rock burst criteria and control based on an abutment-stress-transfer model in deep coal roadways," *Energy Science & Engineering*, vol. 8, no. 8, pp. 2966–2975, 2020.

[18] L. Dai, Y. Pan, Z. Li et al., "Quantitative mechanism of roadway rockbursts in deep extra-thick coal seams: theory and case histories," *Tunnelling and Underground Space Technology*, vol. 111, Article ID 103861, 2021.

[19] M. Gao, Y. He, D. Xu, and X. Yu, "A new theoretical model of rock burst-prone roadway support and its application," *Geofluids*, vol. 2021, Article ID 5549875, 11 pages, 2021.

[20] J. K. Jiao and W. J. Ju, "Burst failure mechanism of roadway anchorage bearing structure under dynamic load disturbance," *Journal of China Coal Society*, vol. 46, pp. 94–105, 2021.

[21] O. Vardar, C. Wei, C. Zhang, and I. Canbulat, "An energy-based quantitative coal burst proneness rating system for development roadways," *Geomechanics and Geophysics for Geo-Energy and Geo-Resources*, vol. 9, no. 1, Article ID 19, 2023.

[22] M. S. Gao, Y. C. Zhao, X. Chen, Q. T. Lu, and A. Liu, "Destruction mechanism of rock burst in mine roadways and their prevention," *Disaster Advances*, vol. 6, pp. 34–43, 2013.

[23] L. Cheng, Y. Zhang, M. Ji, M. Cui, K. Zhang, and M. Zhang, "Theoretical calculation and analysis on the composite rock-bolt bearing structure in burst-prone ground," *Mathematical Problems in Engineering*, vol. 2015, Article ID 434567, 6 pages, 2015.

[24] Q. Wang, H. Ye, N. Li et al., "A study of support characteristics of collaborative reinforce system of u-steel support and anchored cable for roadway under high dynamic stress," *Geofluids*, vol. 2021, Article ID 9881280, 12 pages, 2021.

[25] P. Boresi, K. P. Chong, and J. D. Lee, *Elasticity in Engineering Mechanics*, John Wiley & Sons, Inc., New York, 3rd edition, 2011.

[26] B. H. G. Brady and E. T. Brown, "Energy, mine stability, mine seismicity and rockbursts," in *Rock Mechanics for Underground Mining*, pp. 271–311, Springer, Dordrecht, 3rd edition, 2006.

[27] J. He, *Research of mining dynamic loading effect and its induced rock burst in coal mine*, Dissertation, China University of Mining and Technology, Xuzhou, pp. 29-30, 2013.

[28] Z.-Y. Wang, L.-M. Dou, and G.-F. Wang, "Mechanism analysis of roadway rockbursts induced by dynamic mining loading and its application," *Energies*, vol. 11, no. 9, Article ID 2313, 2018.

[29] Y. S. Zhao, Z. C. Feng, and Z. J. Wan, "Least energy principle of dynamical failure of rock mass," *Chinese Journal of Rock Mechanics and Engineering*, vol. 22, no. 11, pp. 1781–1783, 2003.

[30] J. He, L.-M. Dou, A.-Y. Cao, S.-Y. Gong, and J.-W. Lü, "Rock burst induced by roof breakage and its prevention," *Journal of Central South University*, vol. 19, no. 4, pp. 1086–1091, 2012.

[31] Z.-L. Li, X.-Q. He, L.-M. Dou, D.-Z. Song, and G.-F. Wang, "Numerical investigation of load shedding and rockburst reduction effects of top-coal caving mining in thick coal seams," *International Journal of Rock Mechanics and Mining Sciences*, vol. 110, pp. 266–278, 2018.

[32] H. Liu, B. Zhang, X. Li et al., "Research on roof damage mechanism and control technology of gob-side entry retaining under close distance gob," *Engineering Failure Analysis*, vol. 138, no. 5, Article ID 106331, 2022.

[33] G. Wang, L. Dou, Z. Li, S. Gong, J. He, and W. Cai, "Anti-impact abilities calculation and feasibility analysis of seismic reverse for supporting Chinese," *Chinese Journal of Rock Mechanics and Engineering*, vol. 34, pp. 4125–4131, 2015.

[34] X. Li, S. Chen, S. Wang, M. Zhao, and H. Liu, "Study on in situ stress distribution law of the deep mine: taking Linyi mining area as an example," *Advances in Materials Science and Engineering*, vol. 2021, Article ID 5594181, 11 pages, 2021.

[35] B. Wang, M. He, and Y. Qiao, "Resistance behaviour of constant-resistance-large-deformation bolt considering surrounding rock pressure," *International Journal of Rock Mechanics and Mining Sciences*, vol. 137, Article ID 104511, 2021.

[36] L. Dai, Y. Pan, A. Wang, Y. Xiao, and X. Ma, "Experimental study on the self-protection performance of anchor bolts with energy-absorbing tails," *Rock Mechanics and Rock Engineering*, vol. 53, no. 5, pp. 2249–2263, 2020.

[37] "Coal industry standard of People's Republic of China, resin anchor bolts—Part 1: Capsules," Coal Industry Standard of People's Republic of China, Beijing, pp. 2-3, 2010.

[38] D. Xu, M. Gao, and X. Yu, "Dynamic response characteristics of roadway surrounding rock and the support system and rock burst prevention technology for coal mines," *Energies*, vol. 15, no. 22, Article ID 8662, 2022.

[39] F. Gong, Z. He, and Q. Jiang, "Internal mechanism of reducing rockburst proneness of rock under high stress by real-time drilling pressure relief," *Rock Mechanics and Rock Engineering*, vol. 55, no. 8, pp. 5063–5081, 2022.

[40] Y. Sun, X. Zhang, and H. Xu, "Research on rock burst control mechanism of deep buried tunnel using surrounding rock modification theory," *Shock and Vibration*, vol. 2022, Article ID 5057665, 13 pages, 2022.